Consequences of μ-τ reflection symmetry for 3 + 1 neutrino mixing

Kaustav Chakraborty,[1,2,*] Srubabati Goswami,[1,†] and Biswajit Karmakar[1,‡]

[1]*Theoretical Physics Division, Physical Research Laboratory, Ahmedabad - 380009, India*
[2]*Discipline of Physics, Indian Institute of Technology, Gandhinagar - 382355, India*

We investigate the consequences of μ-τ reflection symmetry in presence of a light sterile neutrino for the 3 + 1 neutrino mixing scheme. We discuss the implications of total μ-τ reflection symmetry as well as partial μ-τ reflection symmetry. For the total μ-τ reflection symmetry we find that values of θ_{23} and δ remain confined near $\pi/4$ and $\pm\pi/2$, respectively. The current allowed region for θ_{23} and δ in case of inverted hierarchy lies outside the area preferred by the total μ-τ reflection symmetry. However, interesting predictions on the neutrino mixing angles and Dirac CP violating phases are obtained considering partial μ-τ reflection symmetry. We obtain predictive correlations between the neutrino mixing angle θ_{23} and Dirac CP phase δ and study the testability of these correlations at the future long baseline experiment DUNE. We find that while the imposition of μ-τ reflection symmetry in the first column admits both normal and inverted neutrino mass hierarchy, demanding μ-τ reflection symmetry for the second column excludes the inverted hierarchy. Interestingly, the sterile mixing angle θ_{34} gets tightly constrained considering the μ-τ reflection symmetry in the fourth column. We also study the implications of μ-τ reflection symmetry for the Majorana phases and neutrinoless double beta decay in the 3 + 1 scenario.

I. INTRODUCTION

Over the past years nonzero neutrino masses and mixings have been well established by several neutrino oscillation experiments and most of the parameters have been measured with considerable precision. The parameters governing the three generation neutrino oscillation phenomena are the three mixing angles (namely, solar mixing angle θ_{12}, atmospheric mixing angle θ_{23} and rector mixing angle θ_{13}), two mass-squared differences (namely, solar mass-squared difference $\Delta m_{\text{sol}}^2 = m_2^2 - m_1^2$ and atmospheric mass-squared difference $\Delta m_{\text{atm}}^2 = m_3^2 - m_1^2$) and Dirac CP phase δ. Among these, the unknown parameters at the present epoch are (a) the octant of θ_{23}, i.e., $\theta_{23} < 45°$ (lower octant, LO) or $\theta_{23} > 45°$ (higher octant, HO), (b) sign of Δm_{atm}^2, i.e., mass ordering of neutrinos where $\Delta m_{\text{atm}}^2 > 0$ is called normal hierarchy (NH), $\Delta m_{\text{atm}}^2 < 0$ is called inverted hierarchy (IH) and (c) magnitude of Dirac CP phase δ. Oscillation experiments are sensitive to the mass-squared differences but the absolute mass scale of the

light neutrinos are still unknown and there exists only an upper bound on the sum of absolute neutrino masses $\sum_{i=1}^3 m_i \leq 0.17$ eV [1], from cosmology. From oretical perspective, lots of effort have been exercised in last few decades to realize the observed neutrino mixing pattern. In this regard, many discrete flavor symmetry groups were exploited to understand the dynamics of this mixing pattern in the lepton sector by extending the Standard Model gauge group with some additional symmetry. A review on lepton masses and mixing based on such discrete groups can be found for instance in [2–6].

The observational data guided by $\theta_{23} \approx 45°$ is indicative of a simple μ-τ flavor symmetry. The simplest realization of such μ-τ flavor symmetry is known as μ-τ permutation symmetry. Conventionally, μ-τ permutation symmetry is identified with the transformation given by $\nu_e \to \nu_e$, $\nu_\mu \to \nu_\tau$, and $\nu_\tau \to \nu_\mu$, imposition of which leaves the neutrino mass term unaltered. There exists a plethora of models based on various discrete flavor symmetry groups possessing an underlying μ-τ permutation symmetry. For example, with $\sin^2 \theta_{23} = 1/2, \sin^2 \theta_{12} = 1/3$, and $\sin^2 \theta_{13} = 0$ one can obtain a special mixing pattern known as tribimaximal mixing [7].[1] Such first approximations of the neutrino data can easily be reproduced with discrete flavor group like A_4, S_4 etc., [3,8–11]. For a review on μ-τ

---

[1]Here it is worth mentioning that mixing schemes like trimaximal, bimaximal, golden ratio also depends upon similar hypothesis of the lepton mixing matrix.

flavor symmetry and its phenomenological implications see [12].

Present oscillation data, particularly after precise measurement of nonzero θ_{13} ($\sim 8°-9°$), however rules out exact μ-τ permutation symmetry and motivates one to go beyond this symmetry. In this context, a particular variant of μ-τ flavor symmetry, known as μ-τ reflection symmetry, which predicts both nonzero θ_{13} as well as maximal CP violation as hinted by current observation is worth studying. This idea, based on the cumulative operation of μ-τ flavor exchange and CP transformation was first coined by Harrison and Scott [13]. This can be expressed as the transformation: $\nu_e \rightarrow \nu_e^c$, $\nu_\mu \rightarrow \nu_\tau^c$ and $\nu_\tau \rightarrow \nu_\mu^c$ ("c" stands for the charge conjugation of the corresponding neutrino field), under which the neutrino mass term remains unchanged. As μ-τ reflection symmetry is still phenomenologically viable, model building with such underlying symmetry in neutrino sector became popular in recent times, particularly with three active neutrinos [3–6,14]. The predictions of the μ-τ reflection symmetry for three neutrino mixing can be summarized as follows: (A) $\theta_{23} = 45°$, $\theta_{13} = 0°$ or (B) $\theta_{23} = 45°$, $\delta = 90°$ or $270°$. Case A is disfavored after measurement on nonzero θ_{13} by reactor experiments [15]. On the other hand, case B is disfavored by the current data which points towards nonmaximal θ_{23}. The consequence of such a symmetry for three neutrino mixing scheme have been discussed in several occasions [16–31]. In particular, breaking of μ-τ reflection symmetry to generate the deviation from maximal θ_{23} have been considered in [25–31]. Another theoretically motivated [32–36] scenario called partial μ-τ reflection symmetry have also been studied to generate deviations from the above values and which resulted in interesting correlations [37,38] between mixing parameters. All the discrete subgroups of $SU(3)$ belonging to class C or D and having three dimensional irreducible representation can lead to the realisation of partial μ-τ reflection symmetry [34]. Discrete subgroups of $U(3)$ can also serve the same purpose, see [33,34] for discussion.

In addition to three active neutrinos, there may exist a light sterile neutrino (Standard Model gauge singlets) at the eV scale (for a review see [39]) which can address anomalies in $\nu_\mu \rightarrow \nu_e$ oscillations observed in some short-baseline neutrino oscillation experiments. Initially the anomaly was found in the antineutrino flux measurement of LSND accelerator experiment [40,41] at Los Alamos which was subsequently confirmed by MiniBooNE [42] (a short baseline experiment at Fermilab). Very recently MiniBooNE experiment again refurbished their earlier results with ν_e appearance data reinstating the presence of a light sterile neutrino [43]. Results from few experiments like gallium solar experiments [44–46] with artificial neutrino sources, reactor neutrino experiments [47,48] with recalculated fluxes also support the hypothesis of at least one sterile neutrino. In this context the $3 + 1$ scenario [49]

consisting of three active neutrinos and mixing with one eV scale sterile neutrino is considered to be most viable [50,51]. Here, we have to keep in mind that inclusion of sterile neutrinos must face tight cosmological hurdles coming from the cosmic microwave background observations, big bang nucleosynthesis, and large scale structures. Although fully thermalized sterile neutrinos with mass ~ 1 eV are not cosmologically safe, they can still be generated via "secret interactions" [52–54]. For a brief review on eV scale sterile neutrinos see [55]. Despite many constrains as well as tension between disappearance and appearance data from oscillation experiments the sterile neutrino conjecture is still a topic of intense research.

In the context of $3 + 1$ neutrino mixing exact μ-τ permutation symmetry would still give θ_{13} zero. Studies have been accomplished in the literature examining the possible role of active-sterile mixing in generating a breaking of this symmetry starting from a μ-τ symmetric 3×3 neutrino mass matrix [28,56–61]. In this paper we concentrate on the ramifications of μ-τ reflection symmetry for the 4×4 neutrino mass matrix in presence of one sterile neutrino. We study the consequences of total as well as partial μ-τ reflection symmetry in the $3 + 1$ framework and obtain predictions and correlations between different parameters. We also formulate the 4×4 neutrino mass matrix which can give rise to such a μ-τ reflection symmetry. Further we study the experimental consequences of μ-τ reflection symmetry at the future long baseline neutrino oscillations experiment DUNE. In addition we discuss the implications of μ-τ reflection symmetry for Majorana phases and neutrinoless double β decay.

Rest of this paper is organized as follows. In Sec. II we first construct the generic structure of the 4×4 mass matrix which can give rise to μ-τ reflection symmetry for sterile neutrinos. In the next section, we find the correlation among the active and sterile mixing angles and Dirac CP phases. In Sec. IV we study the experimental implications of such μ-τ reflection symmetry for DUNE experiment and also calculate the effective neutrino mass which can be probed through neutrinoless double β decay experiments. Then finally in Sec. V we summarize the findings.

II. μ-τ REFLECTION SYMMETRY FOR 3+1 NEUTRINO MIXING

Guided by the atmospheric neutrino data, the μ-τ reflection symmetry was first proposed for 3-generation neutrino mixing back in 2002 [13,16]. Under such symmetry the elements of lepton mixing matrix satisfy:

$$|U_{\mu i}| = |U_{\tau i}| \quad \text{where } i = 1, 2, 3. \tag{1}$$

This indicates that the moduli of μ and τ flavor elements of the 3×3 neutrino mixing matrix are equal. With these constraints, the neutrino mixing matrix can be parametrized as [13,16]

$$U_0 = \begin{pmatrix} u_1 & u_2 & u_3 \\ v_1 & v_2 & v_3 \\ v_1^* & v_2^* & v_3^* \end{pmatrix}, \qquad (2)$$

where the entries in the first row, u_i's are real (and non-negative).[2] v_i satisfy the orthogonality condition $\mathrm{Re}(v_j v_k^*) = \delta_{jk} - u_k u_k$ [12]. In [16], it was argued that the mass matrix leading to the mixing matrix given in Eq. (2) can be written as

$$\mathcal{M}_0 = \begin{pmatrix} a & d & d^* \\ d & c & b \\ d^* & b & c^* \end{pmatrix}, \qquad (3)$$

where a, b are real and d, c are complex parameters. As a consequence of the symmetry given in Eqs. (1)–(3), we obtain the predictions for maximal $\theta_{23} = 45°$ and $\delta = 90°$ or $270°$ in the basis where the charged leptons are considered to be diagonal. This scheme however still leaves room for nonzero θ_{13}. Several attempts were made in this direction to explain correct mixing (for three active neutrinos) with μ-τ reflection symmetry and to study their origin and consequences in various scenarios [21,24–26, 31,33,63–73].

Although, μ-τ reflection symmetry is well studied for three active neutrinos, it lacks a comprehensive study considering sterile neutrinos. Now such a mixing scheme can easily be extended for a $3 + 1$ scenario incorporating sterile neutrinos. Under such circumstances, the 4×4 neutrino mixing matrix can be parametrized as

$$U = \begin{pmatrix} u_1 & u_2 & u_3 & u_4 \\ v_1 & v_2 & v_3 & v_4 \\ v_1^* & v_2^* & v_3^* & v_4^* \\ w_1 & w_2 & w_3 & w_4 \end{pmatrix}, \qquad (4)$$

where u_i, w_i are real but v_i are complex. Within this extended scenario, the mass matrix can now be written as

$$\mathcal{M} = \begin{pmatrix} a & d & d^* & e \\ d & c & b & f \\ d^* & b & c^* & f^* \\ e & f & f^* & g \end{pmatrix}, \qquad (5)$$

where a, b, e, g are real and d, c, f are complex parameters. Such a complex symmetric mass matrix can be obtained from the Lagrangian

$$\mathcal{L}_{\mathrm{mass}} = \frac{1}{2} \nu_L^T C^{-1} \mathcal{M}_\nu \nu_L + \mathrm{H.c.} \qquad (6)$$

with $U^T \mathcal{M}_\nu U = \hat{m} \equiv \mathrm{diag}(m_1, m_2, m_3, m_4)$, where m_j's are the real positive mass eigenvalues. Here the matrix $\mathcal{M}$ is characterized by the transformation

$$S\mathcal{M}_\nu S = \mathcal{M}_\nu^* \quad \text{with} \quad S = \begin{pmatrix} 1 & 0 & 0 & 0 \\ 0 & 0 & 1 & 0 \\ 0 & 1 & 0 & 0 \\ 0 & 0 & 0 & 1 \end{pmatrix}, \qquad (7)$$

and respects the mixing matrix given in Eq. (4). To verify this compatibility between the neutrino mixing and mass matrix let us first write mixing matrix as $U = (c_1, c_2, c_3, c_4)$ with column vectors c_j. Then using the diagonalization relation $U^T \mathcal{M}_\nu U = \mathrm{diag}(m_1, m_2, m_3, m_4)$ one can write

$$\mathcal{M}_\nu c_j = m_j c_j^*. \qquad (8)$$

Now, using Eq. (7), we find

$$\mathcal{M}_\nu (S c_j^*) = m_j (S c_j^*)^*. \qquad (9)$$

Following the above equation, one can therefore find another diagonalizing matrix, $U' = SU^*$. Now it can be shown that if both U and U' satisfy the diagonalization relation $U^T \mathcal{M}_\nu U = \mathrm{diag}(m_1, m_2, m_3, m_4)$ with nondegenerate mass eigenvalues, then there exists a diagonal unitary matrix X such that

$$SU^* = UX, \qquad (10)$$

here X_{jj} is an arbitrary phase factor for $m_j = 0$ and $X = \pm 1$ for $m_j \neq 0$. Therefore the constraint obtained in Eq. (10) leads to[3]

$$|U_{\mu i}| = |U_{\tau i}| \quad \text{where} \quad i = 1, 2, 3, 4. \qquad (11)$$

The above equation can also be verified in an alternate way. Let us first define an Hermitian matrix as,

$$H = \mathcal{M}_\nu^* \mathcal{M}_\nu \qquad (12)$$

considering the form of $\mathcal{M}_\nu$ given in Eq. (5) one can easily find

$$H_{\mu\mu} = H_{\tau\tau} \quad \text{and} \quad H_{e\mu} = H_{e\tau}^*, \qquad H_{s\mu} = H_{s\tau}^*. \qquad (13)$$

Now, one can write the diagonalization relation in this case as: $H_{\alpha\beta} = U_{\alpha i} \hat{m}_{ij}^2 U_{j\beta}^\dagger$. Hence using Eq. (13) we get

---

[2]Various implications of Majorana phases under such symmetry can be found in [62].

[3]Following the same approach for 3ν in [16].

$$\sum_{i=1}^{4} \hat{m}_{ii}^2 |U_{\mu i}|^2 = \sum_{i=1}^{4} \hat{m}_{ii}^2 |U_{\tau i}|^2$$

which follows only if masses are degenerate or $|U_{\mu i}| = |U_{\tau i}|$ [16]. Therefore, it is now clear to us that the mass matrix given in Eq. (5) actually leads to a mixing matrix of the form in Eq. (4). In the following section we discuss the consequences of this μ-τ reflection symmetry involving the active and sterile mixing angles and phases in details.

It is important to note that the mixing matrix given in Eq. (2) should correspond to the standard neutrino mixing matrix U_{PMNS} for three generation case. Now, depending upon the choice of the arbitrary phase factor X given in Eq. (10) the Majorana phases can be fixed in the context of μ-τ reflection symmetry. With the choice of $X_{ii} = 1$ or -1 the Majorana phases are fixed at 0° or 90° [12,25]. Such fixed values of phases can have implication for neutrinoless double beta decay which will be discussed later.

III. CONSTRAINING 3 + 1 NEUTRINO MIXING WITH μ-τ REFLECTION SYMMETRY

For $3 + 1$ neutrino mixing scenario the neutrino mixing matrix U can be written in terms of a 4×4 unitary matrix. This unitary matrix can be parametrized by three active neutrino mixing angles $\theta_{13}, \theta_{12}, \theta_{23}$ and three more angles originating from active-sterile mixing, namely, θ_{14}, θ_{24}, and θ_{34}. It will also contain three Dirac CP violating phases, such as, δ, δ_{14}, and δ_{24}. Hence this 4×4 unitary Pontecorvo–Maki–Nakagawa–Sakata (PMNS) matrix U can be given by

$$U = R_{34}\tilde{R}_{24}\tilde{R}_{14}R_{23}\tilde{R}_{13}R_{12}, \tag{14}$$

where the rotation matrices R and $\tilde{R}$'s can be written as

$$R_{34} = \begin{pmatrix} 1 & 0 & 0 & 0 \\ 0 & 1 & 0 & 0 \\ 0 & 0 & c_{34} & s_{34} \\ 0 & 0 & -s_{34} & c_{34} \end{pmatrix}, \qquad \tilde{R}_{24} = \begin{pmatrix} 1 & 0 & 0 & 0 \\ 0 & c_{24} & 0 & s_{24}e^{-i\delta_{24}} \\ 0 & 0 & 1 & 0 \\ 0 & -s_{24}e^{i\delta_{24}} & 0 & c_{24} \end{pmatrix},$$

$$\tilde{R}_{14} = \begin{pmatrix} c_{14} & 0 & 0 & s_{14}e^{-i\delta_{14}} \\ 0 & 1 & 0 & 0 \\ 0 & 0 & 1 & 0 \\ -s_{14}e^{-i\delta_{14}} & 0 & 0 & c_{14} \end{pmatrix}, \qquad R_{23} = \begin{pmatrix} 1 & 0 & 0 & 0 \\ 0 & c_{23} & s_{23} & 0 \\ 0 & -s_{23} & c_{23} & 0 \\ 0 & 0 & 0 & 1 \end{pmatrix},$$

$$\tilde{R}_{13} = \begin{pmatrix} c_{13} & 0 & s_{13}e^{-i\delta} & 0 \\ 0 & 1 & 0 & 0 \\ -s_{13}e^{i\delta} & 0 & c_{13} & 0 \\ 0 & 0 & 0 & 1 \end{pmatrix}, \qquad R_{12} = \begin{pmatrix} c_{12} & s_{12} & 0 & 0 \\ -s_{12} & c_{12} & 0 & 0 \\ 0 & 0 & 1 & 0 \\ 0 & 0 & 0 & 1 \end{pmatrix}. \tag{15}$$

Along with the parametrization defined in Eq. (14), there also exists a diagonal phase matrix, $P = \mathrm{diag}(1, e^{i\alpha}, e^{i(\beta+\delta)}, e^{i(\gamma+\delta_{14})})$, where α, β and γ are the Majorana phases. The PMNS matrix with the Majorana phases takes the form as

$$U = R_{34}\tilde{R}_{24}\tilde{R}_{14}R_{23}\tilde{R}_{13}R_{12}P, \tag{16}$$

Note that, the correspondence of the mixing matrix in Eq. (4) along with the diagonal phase matrix P in Eq. (16) implies that the Majorana phases are zero or $\pm\frac{\pi}{2}$. However, in light of Eq. (1) this diagonal phase matrix does not play any role in the present analysis. But they can play role in neutrinoless double β decay which will be discussed in Sec. IV. Following these conditions, one can obtain four different equalities among six mixing angles and three Dirac CP violating phases. To keep the present analysis

simple, first we have assumed the sterile Dirac CP violating phases (δ_{14} and δ_{24}) to be zero. For this case, $\delta_{14} = \delta_{24} = 0°$, from Eq. (1) these four correlations can be written as,

$$\cos\delta = \frac{(a_1^2 + b_1^2) - (c_1^2 + d_1^2)}{2(c_1 d_1 - a_1 b_1)} \quad (\text{for } |U_{\mu 1}| = |U_{\tau 1}|) \tag{17}$$

$$\cos\delta = \frac{(a_2^2 + b_2^2) - (c_2^2 + d_2^2)}{2(a_2 b_2 - c_2 d_2)} \quad (\text{for } |U_{\mu 2}| = |U_{\tau 2}|) \tag{18}$$

$$\cos\delta = \frac{(a_3^2 + b_3^2) - (c_3^2 + d_3^2)}{2(a_3 b_3 - c_3 d_3)} \quad (\text{for } |U_{\mu 3}| = |U_{\tau 3}|) \tag{19}$$

$$\tan^2\theta_{24} = \sin^2\theta_{34} \quad (\text{for } |U_{\mu 4}| = |U_{\tau 4}|) \tag{20}$$

where

$$a_1 = (c_{12}s_{13}s_{23}s_{24}s_{34} - c_{12}c_{23}c_{34}s_{13}), \qquad b_1 = (c_{34}s_{12}s_{23} - c_{12}c_{13}c_{24}s_{14}s_{34} + c_{23}s_{12}s_{24}s_{34})$$

$$c_1 = (c_{23}c_{24}s_{12} + c_{12}c_{13}s_{14}s_{24}), \qquad d_1 = (c_{12}c_{24}s_{13}s_{23}), \qquad a_2 = c_{12}(c_{34}s_{23} + c_{23}s_{24}s_{34}) + s_{12}c_{13}c_{24}s_{14}s_{34}$$

$$b_2 = s_{12}(s_{13}s_{23}s_{24}s_{34} - c_{23}c_{34}s_{13}), \qquad c_2 = (c_{12}c_{23}c_{24} - s_{12}c_{13}s_{14}s_{24}), \qquad d_2 = s_{12}c_{24}s_{13}s_{23}$$

$$a_3 = c_{13}(c_{23}c_{34} - s_{23}s_{24}s_{34}), \qquad b_3 = c_{24}s_{13}s_{14}s_{34}, \qquad c_3 = s_{13}s_{14}s_{24} \quad \text{and} \quad d_3 = c_{13}c_{24}s_{23}. \tag{21}$$

Here, the first three equalities enable us to study the correlation among the mixing angles θ_{12}, θ_{23}, θ_{13}, θ_{14}, θ_{24}, θ_{34} and Dirac CP phase δ whereas the fourth relation yields a crucial correlation between the two sterile mixing angles θ_{24} and θ_{34}. For δ_{14} & $\delta_{24} \neq 0°$, such compact expressions cannot be obtained. However, in our numerical analysis we have studied the effect of inclusion of these phases. When the sterile mixing angles (θ_{14}, θ_{24}, θ_{34}) are taken to be zero, the correlations obtained in Eqs. (17)–(21) reduces to the three neutrino mixing scenarios studied in [33,37,38,74,75]. Below we study the various correlations between the parameters due to Eqs. (17)–(21). We find that the phenomenologically interesting correlations are between $\theta_{23} - \delta$ and $\theta_{24} - \theta_{34}$. Since the other sterile mixing angles are already restricted to a narrow range, no other important correlations are obtained.

A. Total μ-τ Symmetry

In this subsection we present the results assuming μ-τ reflection symmetry to be valid for all the four columns simultaneously; we call this as the total μ-τ reflection symmetry. The magenta shaded region in Fig. 1 represents the allowed region for total μ-τ symmetry for $3+1$ neutrino scenario in θ_{23}-δ plane. The analysis is performed by varying the other mixing parameters in their 3σ range as in Table I and the sterile CP phases δ_{14} and δ_{24} between
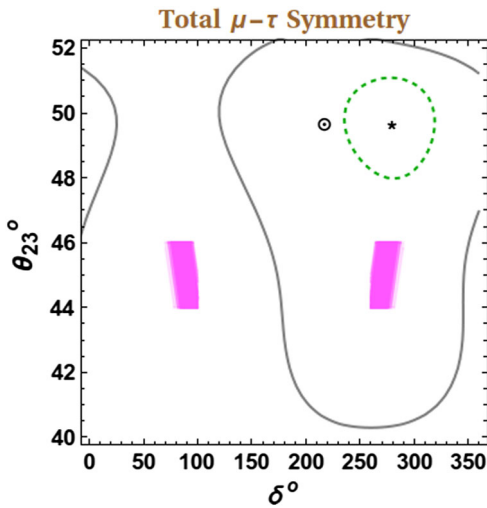
0° and 360°.[4] The grey solid and green dashed contours denote the currently allowed parameter space for NH and IH respectively in this and the subsequent figures. The application of the total μ-τ symmetry significantly restricts the parameters θ_{23} and δ. θ_{23} is primarily restricted around the maximal while δ falls in the close vicinity of 90° and 270°. Comparing the results with 3 neutrino scenario [32,33] where θ_{23} is strictly restricted to be maximal and δ to 90° and 270° we conclude that the involvement of the sterile mixing angles and phases lead to slight deviations in θ_{23} and δ from their 3 generation predictions. However, the current global fit results from [76] suggests that the best fit for θ_{23} is 49.5° for both normal and inverted hierarchies. Thus, even with inclusion of sterile neutrinos, total μ-τ reflection symmetry cannot explain the current best fit. This motivates us to consider the partial μ-τ reflection symmetry for the $3+1$ scenario.

B. Partial μ-τ Reflection Symmetry

In this section we discuss the implications partial μ-τ reflection symmetry which implies that the condition $|U_{\mu i}| = |U_{\tau i}|$ is satisfied for individual columns.

1. $|U_{\mu 1}| = |U_{\tau 1}|$

The correlation obtained from the equality $|U_{\mu 1}| = |U_{\tau 1}|$ has been plotted in the θ_{23}-δ plane in Fig. 2. The left panel with red contours in Fig. 2 represents the case with sterile phases δ_{14} and δ_{24} taken to be zero while the right panel with blue contours denotes the case with δ_{14} and δ_{24} to be nonzero. In these panels, the grey continuous and green dashed contours represent 3σ allowed range in the θ_{23}-δ plane and the $\odot$ and $\star$ represents the best-fit values for normal and inverted neutrino mass hierarchy respectively.[5] The interesting result obtained from these correlations are the range of δ allowed by the μ-τ reflection symmetry. In this case the CP conserving values of δ are ruled out and preference is seen for maximal CP violation. This points towards an important consequence of μ-τ reflection symmetry i.e., if μ-τ reflection symmetry is true for the first column of lepton mixing matrix CP violation is implied. The recent global fit [76] result also points towards the maximal CP violation with preference for $\delta \sim 270°$.

Total μ−τ Symmetry

FIG. 1.   Allowed region for total μ-τ symmetry for $3+1$ neutrino scenario. Here the other mixing parameters are varied within 3σ range [76–78]

---

[4]Here (and in the rest of the analysis, unless otherwise mentioned) we vary both δ_{14} and δ_{24} between 0° and 360°.

[5]Similar descriptions are also true for the subsequent figures for $|U_{\mu 2}| = |U_{\tau 2}|$ and $|U_{\mu 3}| = |U_{\tau 3}|$.
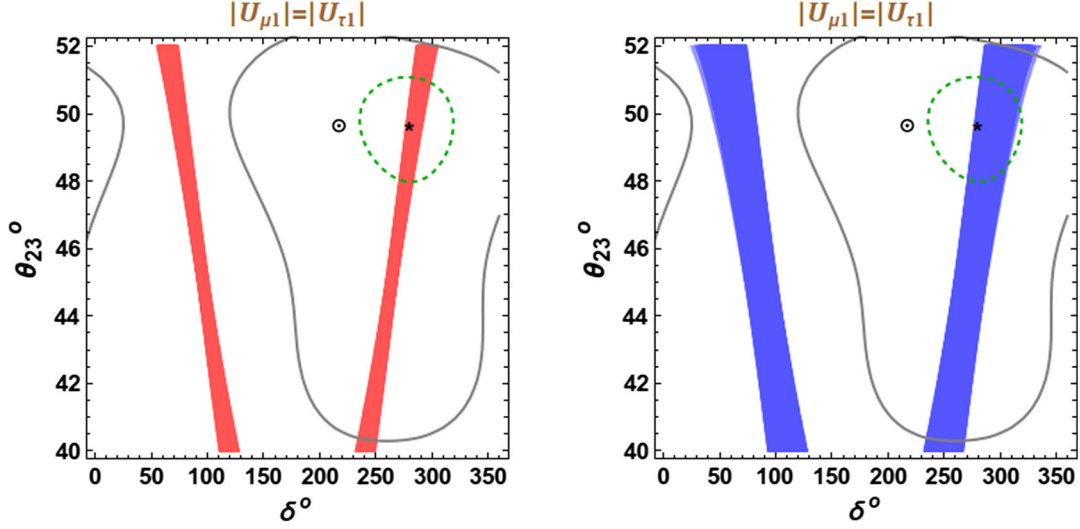
FIG. 2. Correlation between θ_{23} and Dirac CP phase δ for $|U_{\mu 1}| = |U_{\tau 1}|$ with $\delta_{14}, \delta_{24} = 0°$ (left panel) and $\delta_{14}, \delta_{24} \neq 0°$ (right panel) respectively. Here all other mixing parameters are varied within their 3σ range as given in Table I. The continuous and dashed contours represent 3σ allowed range in the θ_{23}-δ plane and the $\odot$ and $\star$ represent the best-fit values for normal and inverted neutrino mass hierarchy respectively.

From both these panels it is clear that under μ-τ reflection symmetry in the first column of lepton mixing matrix, inverted hierarchy of neutrino mass is a more favored scenario given the current best-fit values, this is true with or without the involvement of sterile CP phases (δ_{14}, δ_{24}). The inclusion of the sterile CP phases δ_{14}, δ_{24} predicts slightly larger allowed range for δ.

2. $|U_{\mu 2}| = |U_{\tau 2}|$

μ-τ reflection symmetry in the second column of lepton mixing matrix (given by $|U_{\mu 2}| = |U_{\tau 2}|$) is plotted in Fig. 3.

It is seen from the left panel of this figure that this symmetry disfavors $\delta = 0°$ while $\delta = 180°$ is allowed from the correlation for the current θ_{23} range when sterile CP phases are zero. The presence of the sterile CP phases δ_{14}, δ_{24} predicts slightly larger allowed range for both θ_{23} and δ, and in presence of these phases, both $\delta = 0°$ and $\delta = 180°$ become admissible unlike the previous case in Fig. 2. Interestingly the current 3σ global fit contours for inverted hierarchy do not overlap with the allowed region due to μ-τ reflection symmetry in the second column of the lepton mixing matrix with sterile CP phases $\delta_{14} = \delta_{24} = 0°$.
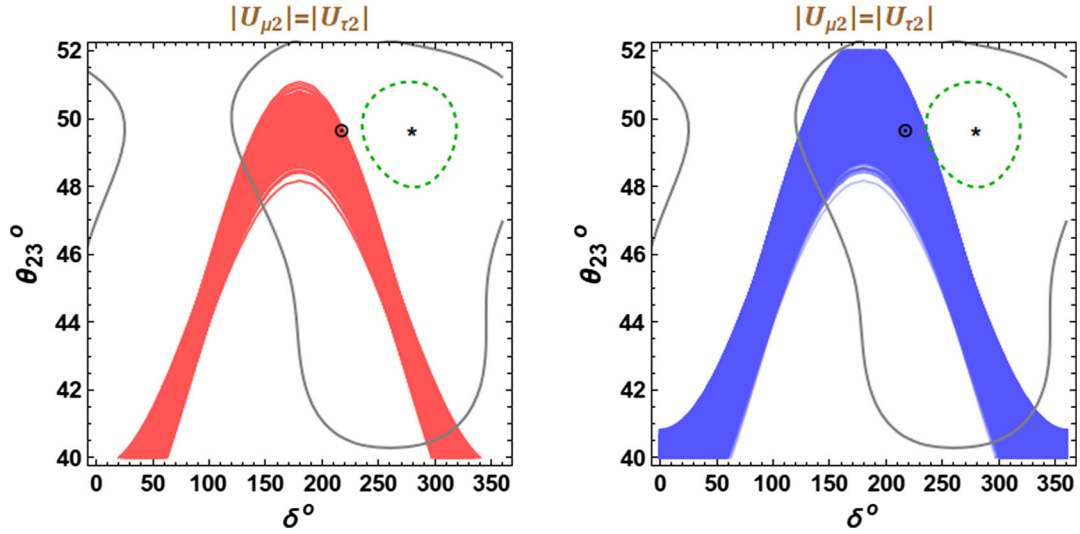

FIG. 3. Correlation between θ_{23} and Dirac CP phase δ for $|U_{\mu 2}| = |U_{\tau 2}|$ with $\delta_{14}, \delta_{24} = 0°$ (left panel) and $\delta_{14}, \delta_{24} \neq 0°$ (right panel) respectively. Here all other mixing parameters are varied within their 3σ range as given in Table I. The continuous and dashed contours represent 3σ allowed range in the θ_{23}-δ plane and the $\odot$ and $\star$ represents the best-fit values for normal and inverted neutrino mass hierarchy respectively.
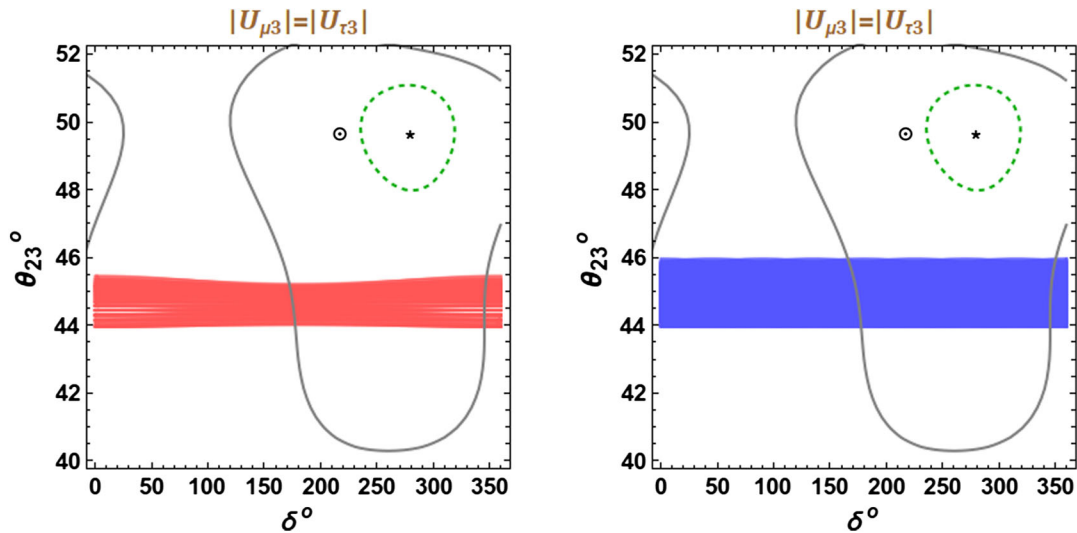
FIG. 4. Correlation between θ_{23} and Dirac CP phase δ for $|U_{\mu3}| = |U_{\tau3}|$ with $\delta_{14}, \delta_{24} = 0°$ (left panel) and δ_{14}, $\delta_{24} \neq 0°$ (right panel) respectively. Here all other mixing parameters are varied within their 3σ range as given in Table I. The continuous and dashed contours represent 3σ allowed range in the θ_{23}-δ plane and the $\odot$ and $\star$ represents the best-fit values for normal and inverted neutrino mass hierarchy respectively.

But, there is a slight overlap between the above specified regions once δ_{14} and δ_{24} are taken nonzero.

3. $|U_{\mu3}| = |U_{\tau3}|$

In Fig. 4 we show the consequence of $|U_{\mu3}| = |U_{\tau3}|$, and it is seen that the allowed value of θ_{23} stays close to maximal with slight deviation within a very narrow range with a preference for the lower octant as given in the left panel of Fig. 4 with $\delta_{14}, \delta_{24} = 0°$. If we introduce the nonzero values for the sterile CP phases ($\delta_{14}, \delta_{24} \neq 0°$), the variation of θ_{23} remains in the vicinity of $45°$ with equal deviations in both lower and higher octants as evident from the right panel of Fig. 4. However, the deviation is not enough to reach the best-fit θ_{23} from current data [76,79,80]. However, if future data from T2K or NOνA give a value closer to maximal θ_{23} (but not exactly maximal) then this scenario can be preferred over the three generation case. Since for the three flavor case, the condition $|U_{\mu3}| = |U_{\tau3}|$ leads to $\theta_{23} = 45°$. However, in presence of sterile neutrinos there is a spread around the maximal value and future measurements of θ_{23} can confirm or falsify if this condition can indeed be satisfied. In this context it is also worthwhile to discuss to what extent future high statistics experiments can determine the octant of θ_{23} close to maximal value. For instance, it was shown in [81] from a combined analysis of DUNE and T2HK that the octant of θ_{23} will remain unresolved for true values in the range $43° - 48.7°$. The maximum allowed range of θ_{23} for $|U_{\mu3}| = |U_{\tau3}|$ in presence of sterile mixing and phases being $44° - 46°$, the octant will remain undetermined in this situation even with the future high statistics experiments.

4. $|U_{\mu4}| = |U_{\tau4}|$

In this $3 + 1$ neutrino framework, the fourth equality $|U_{\mu4}| = |U_{\tau4}|$ establishes a powerful correlation between the two sterile mixing angles θ_{24} and θ_{34}. Here we obtain a one-to-one correspondence between θ_{24} and θ_{34} as given in Eq. (20). Even with the involvement of sterile CP phase this relation remains same as evident from Eq. (11) and (14). This correlation yields a linear dependence between the two sterile mixing angles θ_{24} and θ_{34} as given in Fig. 5. Once we impose the constraints coming from the current
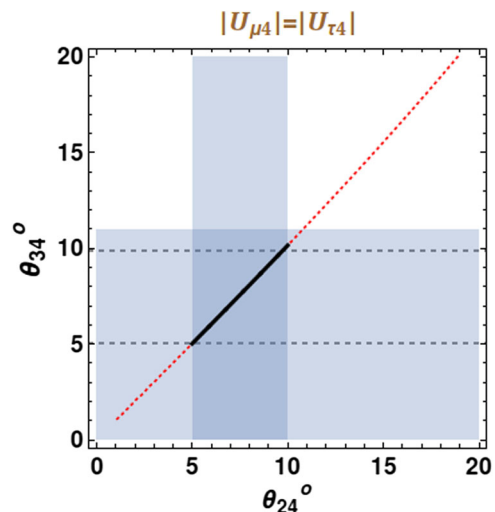

FIG. 5. Constraints on θ_{34} obtained from $|U_{\mu4}| = |U_{\tau4}|$. Here the red dashed line (including the black line) represents this correlation. Shaded regions are current allowed range [78]. Here 3σ allowed range of θ_{24} [78] restricts θ_{34} within the range $4.9°–9.8°$ (as given by the dark black line).

allowed value of θ_{24} [78], the sterile mixing angle θ_{34} becomes restricted from below significantly. Note that so far there only exists a upper limit on θ_{34} [78]. In Fig. 5 we plot this correlation and find that θ_{34} lies within the range $4.9° - 9.8°$ corresponding to the 3σ allowed range of θ_{24} [78]. Therefore, the μ-τ reflection symmetry presented here restricts the sterile mixing angle θ_{34} considerably. The allowed parameter space in the θ_{24}-θ_{34} plane also gets restricted. This is one of the most crucial finding in this μ-τ reflection symmetric framework for $3 + 1$ neutrino scenario. It is to be noted that among the current constraints on sterile mixing angles, the bound on θ_{34} is much weaker, there being only an upper limit on this. The reactor neutrino experiments are sensitive to the mixing matrix element U_{e4}^2 or s_{14}^2 in our parametrization. The short baseline oscillation experiments using appearance channel are sensitive to the product $|U_{e4}|^2|U_{\mu4}^2|$ which contains the product $s_{14}^2 s_{24}^2$. Bounds on θ_{34} have been obtained from atmospheric neutrinos at SuperKamiokande [82], DeepCore detector at Icecube [83], and from neutral current data at MINOS [84], NOνA [85], and T2K [86] experiments. The constraints on θ_{34} from individual experiments are somewhat weaker (in the ballpark of 20°–30°) than what is obtained in the global analysis of [78]. In our analysis the latter has been used. Neutral current events at the DUNE detector can also improve on the bound on θ_{34} coming from a single experiment [87]. The ν_τ appearance channel is also sensitive to θ_{34} and the potential of DUNE experiment to constrain this mixing angle has been studied in [88–90]. Thus it is expected that future data can test this correlation and the allowed parameter space.

These discussions lead us to the inference that partial μ-τ reflection symmetry is more favorable scenario. However it is to be noted that in this scenario the case $|U_{\mu3}| = |U_{\tau3}|$ is disfavored because it fixes θ_{23} around the maximal value. Again, the simultaneous application of equalities $|U_{\mu1}| = |U_{\tau1}|$ and $|U_{\mu2}| = |U_{\tau2}|$ restricts $\theta_{23} \sim 45°$ hence both these equalities cannot be satisfied together. Such experimental constraints do not apply on $|U_{\mu4}| = |U_{\tau4}|$ therefore this equality may still hold. So, the favorable scenarios are

   (i) $|U_{\mu1}| = |U_{\tau1}|$ with $|U_{\mu4}| = |U_{\tau4}|$
   (ii) $|U_{\mu2}| = |U_{\tau2}|$ with $|U_{\mu4}| = |U_{\tau4}|$

IV. EXPERIMENTAL CONSEQUENCES OF μ-τ REFLECTION SYMMETRY

A. Neutrino oscillations experiments

In this section we explore the consequences of partial μ-τ reflection symmetry in the $3 + 1$ scenario for the Deep Underground Neutrino Experiment (DUNE).

1. Experimental and simulation details

DUNE is a proposed future long baseline accelerator experiment which is expected to lead the endeavor in

determination of the unknown neutrino oscillation parameters. The neutrino source for DUNE is proposed to be the Long Baseline Neutrino Facility (LBNF) at Fermilab, which will provide intense 1.2 MW neutrino beams. The detector is a 40 kt liquid Argon detector located at South Dakota with a baseline of 1300 km. The total protons on target (POT) is expected to be 10×10^{21} over a period of 10 years with 5 years each of neutrino and anti-neutrino run. The simulation have been performed using the package General Long Baseline Experiment Simulator (GLoBES) [91,92], and the sterile neutrino effects have been applied using the sterile neutrino engine as described in [93].

To test the correlations at DUNE we define χ^2 as

$$\chi_{\rm tot}^2 = \min_{\xi,\omega}\{\chi_{\rm stat}^2(\omega,\xi) + \chi_{\rm pull}^2(\xi)\}. \tag{22}$$

where, the statistical χ^2 is $\chi_{\rm stat}^2$ while the systematic uncertainties are incorporated by $\chi_{\rm pull}^2$. The later is calculated by the method of pulls with pull variables given by ξ [94–96]. The oscillation parameters $\{\theta_{23}, \theta_{12}, \theta_{13}, \delta_{CP}, \Delta m_{21}^2, \Delta m_{31}^2, \theta_{14}, \theta_{24}, \theta_{34}, \delta_{14}\delta_{24}\}$ are represented by ω. The statistical $\chi_{\rm stat}^2$ is calculated assuming Poisson distribution,

$$\chi_{\rm stat}^2 = \sum_i 2\left(N_i^{\rm test} - N_i^{\rm true} - N_i^{\rm true}\log\frac{N_i^{\rm test}}{N_i^{\rm true}}\right). \tag{23}$$

Here, "i" stands for the number of bins and $N_i^{\rm test}$, $N_i^{\rm true}$ stands for total number of test and true events, respectively. To include the effects of systematics in $N_i^{\rm test}$, pull and "tilt" variables are incorporated as follows:

$$N_i^{(k){\rm test}}(\omega,\xi) = \sum_{k=s,b} N_i^{(k)}(\omega)\left[1 + c_i^{(k){\rm norm}}\xi^{(k){\rm norm}}\right.$$
$$\left. + c_i^{(k){\rm tilt}}\xi^{(k){\rm tilt}}\frac{E_i - \bar{E}}{E_{\rm max} - E_{\rm min}}\right], \tag{24}$$

where $k = s(b)$ represent the signal(background) events. The effect of the pull variable $\xi^{\rm norm}$ ($\xi^{\rm tilt}$) on the number of events are denoted by $c_i^{\rm norm}$ ($c_i^{\rm tilt}$). The bin by bin mean reconstructed energy is represented by E_i where i represents the bin. $E_{\rm min}$, $E_{\rm max}$ and $\bar{E} = (E_{\rm max} + E_{\rm min})/2$ are the minimum energy, maximum energy and the mean energy over this range. The signal normalization uncertainties used are as follows: for $\nu_e/\bar\nu_e$—2% and $\nu_\mu/\bar\nu_\mu$—5%. While the background uncertainties vary from 5% to 20%.

2. μ-τ reflection symmetry at DUNE for $3+1$ neutrino mixing

The consequences of the partial μ-τ reflection symmetry at the experiment is observed by analyzing the confidence region in the θ_{23} (true) vs δ_{CP} (true) plane which remains allowed after the application of the symmetry relations in

TABLE I. The best-fit values and 3σ ranges of the 3 neutrino oscillation parameters [76,77] used in the present analysis and the representative ranges for $3+1$ neutrino mixing [78].

Oscillation parameters	Best-fit	3σ range
θ_{13}	8.6°	8.2°:9.0°
θ_{12}	33.8°	31.6°:36.3°
θ_{23}	49.5	40°:52°
Δm_{21}^2 (eV^2)	7.4×10^{-5}	fixed
$|\Delta m_{31}^2|$ (eV^2)	2.5×10^{-3}	$(2.35:2.65) \times 10^{-3}$
δ	0°:360°	0°:360°

Oscillation parameters	Representative Value	3σ range
Δm_{41}^2 (eV^2)	1	fixed
θ_{14}	9°	4°:10°
θ_{24}	9°	5°:10°
θ_{34}	9°	0°:11°
δ_{14}	–	0°:360°
δ_{24}	–	0°:360°

the test parameters. The approach taken for the numerical analysis can be summarized as follows:

(i) The simulated data for the experiment DUNE are generated for the representative true values of the oscillation parameters as given by the best-fit in Table I excepting for θ_{23} and δ. The true values of these parameters are varied over the range $39° - 51°$ and $0° - 360°$ respectively. The true values of δ_{14} and δ_{24} are taken as 0°.

(ii) The test events are generated by marginalization of the parameters θ_{12}, θ_{13}, $|\Delta m_{31}^2|$, θ_{23}, θ_{14}, θ_{24}, θ_{34} over the range given in Table I subject to the condition embodied in Eq. (17) for the left panel and Eq. (18) for the right panel. The other parameters are held fixed at their true values for calculation

of N_{test}. In this study we have assumed normal hierarchy as the true hierarchy. We have checked that marginalizing over test hierarchy do not have significant effect because the correlations are independent of hierarchy.

(iii) For each true value of θ_{23} and δ the χ^2 is minimized and the allowed regions defined by $\chi^2 \leq \chi_{\text{min}}^2 + \Delta\chi^2$ are plotted corresponding to 1σ, 2σ, and 3σ values of $\Delta\chi^2$.

The experimental consequences at DUNE are presented in Fig. 6. Here the first(second) column represents the correlation $|U_{\mu 1}| = |U_{\tau 1}|$ $(|U_{\mu 2}| = |U_{\tau 2}|)$. The condition $|U_{\mu 4}| = |U_{\tau 4}|$ is also incorporated in both the plots. Each plot consists of 1σ, 2σ, and 3σ confidence regions considering partial μ-τ reflection symmetry which are shaded as blue, grey, and green, respectively. The current 3σ permitted region from NuFIT [76,77] data is drawn with red solid line. The plots show a similar nature as the correlation plots in Fig. 2 and 3, however, the allowed regions are wider which reflects the inclusion of the experimental errors. From the first column of the figure we observe that DUNE can reject the CP conserving values (0°, 180°, and 360°) at 3σ. But when the correlation $|U_{\mu 2}| = |U_{\tau 2}|$ is considered as shown in the right column the CP conserving δ_{CP} values cannot be excluded at 3σ. Note that, some of the areas allowed by the current data are disfavored by applying the correlations. As the correlations predict a range of δ_{CP} given a set of oscillations parameters, the experiments can further constrain the range of δ_{CP} which are allowed by the present oscillation data.

B. Implications for neutrinoless double β decay

Neutrinoless double β decay ($0\nu\beta\beta$) can test whether neutrinos are Majorana particles. This process takes place
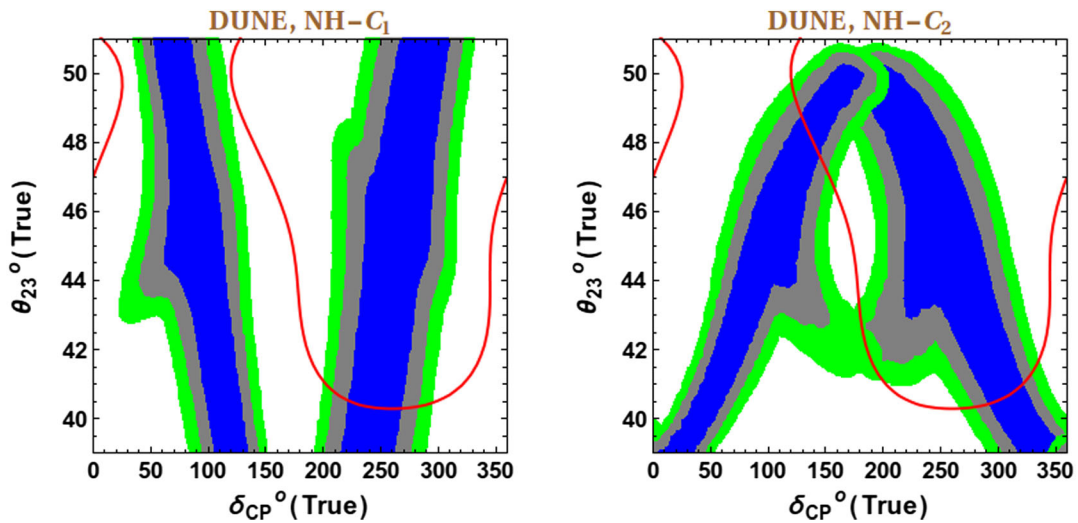

FIG. 6. Experimental constraints on δ_{CP} from the correlations $|U_{\mu 1}| = |U_{\tau 1}|$ and $|U_{\mu 2}| = |U_{\tau 2}|$ for DUNE. The left(right) column indicate correlation $|U_{\mu 1}| = |U_{\tau 1}|$ $(|U_{\mu 2}| = |U_{\tau 2}|)$. The blue, grey, and green shaded regions depict 1σ, 2σ, and 3σ confidence regions, respectively. While the red contours represent the currently allowed 3σ region considering true normal hierarchy.

by emitting two electrons without the emission of the expected antineutrinos as observed in $2\nu\beta\beta$ decay. The half-life ($T_{1/2}$) for the $0\nu\beta\beta$ process is given as,

$$(T_{1/2})^{-1} = \frac{\Gamma_{0\nu\beta\beta}}{\ln 2} = G\left|\frac{M_\nu}{m_e}\right|^2 m_{\beta\beta}^2, \qquad (25)$$

where G contains the lepton phase space integral, m_e is the mass of electron, M_ν is the nuclear matrix element (NME) which takes into consideration all the nuclear structure effects, $m_{\beta\beta}$ stands for the effective neutrino mass and can be expressed as

$$m_{\beta\beta} = |U_{ei}^2 m_i|. \qquad (26)$$

Here m_i are the real positive neutrino mass eigenvalues with $i = 1, 2, 3$ for three generation and $i = 1, 2, 3, 4$ for $3 + 1$ neutrino mixing, respectively.

Null results from several experiments have constrained the lifetimes of $0\nu\beta\beta$. KamLAND-Zen [97] have reported a lifetime of $T_{1/2}(^{136}Xe) > 10.7 \times 10^{25}$ years, GERDA [98] reported as $T_{1/2}(^{76}Ge) > 8 \times 10^{25}$ years, CURCINO and CUORE [99] combined results reported the lifetime as $T_{1/2}(^{130}Te) > 1.5 \times 10^{25}$ years at 90% confidence level. The lower bound on $T_{1/2}$ can be translated to the upper bound of effective neutrino mass ($m_{\beta\beta}$) [100,101]. Using the parametrization of U in Eq. (16), $m_{\beta\beta}$ can be expressed as,

$$m_{\beta\beta} = |m_1 c_{12}^2 c_{13}^2 c_{14}^2 + m_2 s_{12}^2 c_{13}^2 c_{14}^2 e^{i2\alpha}$$
$$+ m_3 s_{13}^2 c_{14}^2 e^{i2\beta} + m_4 s_{14}^2 e^{i2\gamma}|. \qquad (27)$$

For NH (IH) m_1 (m_3) is the lightest neutrino mass eigenstate. All other neutrino mass eigenvalues can be expressed in

terms of the lightest neutrino mass and mass squared differences as follows:

(i) Normal hierarchy (NH): $m_1 < m_2 \ll m_3$ with

$$m_2 = \sqrt{m_1^2 + \Delta m_{\text{sol}}^2}; \qquad m_3 = \sqrt{m_1^2 + \Delta m_{\text{atm}}^2};$$

$$m_4 = \sqrt{m_1^2 + \Delta m_{\text{LSND}}^2}, \qquad (28)$$

(ii) Inverted hierarchy (IH): $m_3 \ll m_1 \approx m_2$ with

$$m_1 = \sqrt{m_3^2 + \Delta m_{\text{atm}}^2};$$

$$m_2 = \sqrt{m_3^2 + \Delta m_{\text{sol}}^2 + \Delta m_{\text{atm}}^2};$$

$$m_4 = \sqrt{m_3^2 + \Delta m_{\text{atm}}^2 + \Delta m_{\text{LSND}}^2}, \qquad (29)$$

where $\Delta m_{\text{sol}}^2 = m_2^2 - m_1^2$, $\Delta m_{\text{atm}}^2 = m_3^2 - m_1^2 (m_1^2 - m_3^2)$ for NH (IH) and $\Delta m_{\text{LSND}}^2 = m_4^2 - m_1^2$.

Predictions for $m_{\beta\beta}$ with respect to the lightest neutrino mass for $3 + 1$ scheme along with the three neutrino case is presented in Fig. 7. The plot in the left panel shows the effective neutrino mass for NH while the right panel is for IH. In generating these plots we have varied the oscillations parameters within their 3σ range as given in Table I with $\Delta m_{\text{LSND}}^2 = 1.7$ eV^2 [78]. In both panels of Fig. 7, the red and blue shaded regions (corresponding to Majorana phases fixed at 0 and 90°, respectively) represents $m_{\beta\beta}$ in presence of μ-τ reflection symmetry in $3 + 1$ neutrino mixing. In the plots (both left and right panel) the area between the black dashed lines at 0.071 eV and 0.161 eV represents the upper limit for $m_{\beta\beta}$ obtained from the combined analysis of GERDA and KamLAND-Zen
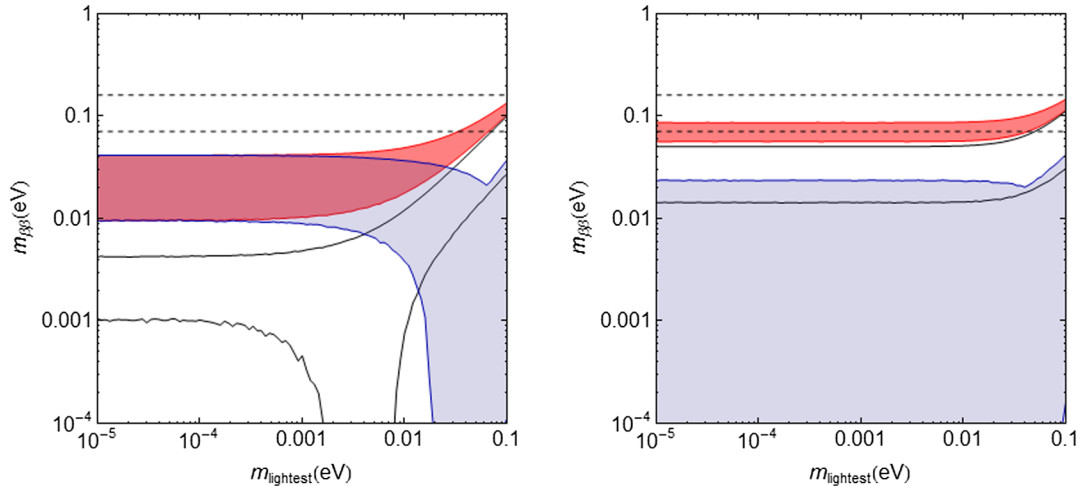

FIG. 7. The effective neutrino mass $m_{\beta\beta}$ for $0\nu\beta\beta$ as a function of the lightest neutrino mass. The left panel shows the effective neutrino mass for NH while the right panel is for IH. The red region represents $m_{\beta\beta}$ in presence of μ-τ reflection symmetry in $3 + 1$ neutrino mixing where the Majorana phases are kept as zero whereas the blue region represents the scenario when all the Majorana phases are fixed at 90°. The areas inside the black solid lines are the 3 neutrino allowed regions. The pair of purple dashed lines at 0.071 eV and 0.161 eV represent the upper limit for $m_{\beta\beta}$ by combined analysis of GERDA and KamLAND-Zen experiments.

experiments. The width in the upper limit of $m_{\beta\beta}$ is present because of the NME uncertainty. For purposes of comparison we also present the three neutrino allowed regions given by the black solid lines in the Fig. 7. Below we discuss from the analytic expression, the allowed regions for $m_{\beta\beta}$ for both hierarchies. The Majorana phases which are of interest to us from the point of view of μ-τ reflection symmetry are 0 and 90°.

(i) Inverted hierarchy:

For inverted hierarchy, the red shaded region corresponds to the case with $\alpha = \beta = \gamma = 0°$. It is seen that $m_{\beta\beta}$ stays almost constant in the range 0.057–0.087 eV till $m_{\text{lightest}} \sim 0.01$ eV, after which there is a slight increase in its value. The width of the band can be ascribed to the variation in the oscillation parameters in their 3σ range. The blue shaded region is obtained for $\alpha = \beta = \gamma = 90°$. It is observed that complete cancellation can be obtained for these values of phases. Thus the two predictions of μ-τ reflection symmetry give drastically different results. Also, the predictions of $m_{\beta\beta}$ for the sterile neutrino case with Majorana phases as 90° are markedly different from the three neutrino case for which there are no cancellation regions. Below we explain these features analytically in different limits of the lightest neutrino mass.

Case 1: When $m_3 \ll m_1 \approx m_2 \approx \sqrt{\Delta m_{\text{atm}}^2}$ and $m_4 \approx \sqrt{\Delta m_{\text{LSND}}^2}$ we find

$$m_{\beta\beta} = \left| \sqrt{\Delta m_{\text{atm}}^2} c_{13}^2 c_{14}^2 (c_{12}^2 + s_{12}^2 e^{i2\alpha}) + \sqrt{\Delta m_{\text{LSND}}^2} s_{14}^2 e^{i2\gamma} \right|. \tag{30}$$

Taking the approximations $c_{13}^2 \sim c_{14}^2 \sim 1$, $s_{12}^2 \sim 0.33$, $c_{12}^2 \sim 0.67$ and $\sqrt{\Delta m_{\text{atm}}^2} \sim 0.05$ eV, $\sqrt{\Delta m_{\text{LSND}}^2} \sim 1$ eV we obtain

$$m_{\beta\beta} = 0.033 + 0.017 e^{i2\alpha} + s_{14}^2 e^{i2\gamma}. \tag{31}$$

For $\alpha = \gamma = 0°$ and s_{14}^2 in the range 0.005-0.03 the above gives $m_{\beta\beta}$ in the range (0.057-0.087) eV which is consistent with the values observed in Fig. 7. On the other hand for $\alpha \sim 90°$ and $\gamma \sim 90°$, one can get cancellations in $m_{\beta\beta}$ for $s_{14}^2 \sim 0.016$. This explains the occurrence of the cancellation regions for this choice of phases.

Case 2: For $m_3 \approx \sqrt{\Delta m_{\text{atm}}^2}$, $m_1 \approx m_2 \approx \sqrt{2\Delta m_{\text{atm}}^2}$, $m_4 \approx \sqrt{\Delta m_{\text{LSND}}^2}$ and we write

$$m_{\beta\beta} = \left| \sqrt{2\Delta m_{\text{atm}}^2} c_{13}^2 c_{14}^2 \left(c_{12}^2 + s_{12}^2 e^{i2\alpha} + \frac{t_{13}^2}{\sqrt{2}} e^{i2\beta} \right) + \sqrt{\Delta m_{\text{LSND}}^2} s_{14}^2 e^{i2\gamma} \right|. \tag{32}$$

Again, utilizing the same values of parameters involved as in Case 1 along with $s_{13}^2 \sim 0.024$ the effective mass can be obtained as

$$m_{\beta\beta} = 0.047 + 0.023 e^{i2\alpha} + 0.001 e^{i2\beta} + s_{14}^2 e^{i2\gamma}. \tag{33}$$

Substituting $\alpha = \beta = \gamma = 0°$ in Eq. (32) one gets $m_{\beta\beta}$ in the range 0.075–0.106 eV which can be seen from the figure for $m_{\text{lightest}} \sim 0.05$ eV.

In this case also cancellations occur for $\alpha = \beta = \gamma \sim 90°$ and $s_{14}^2 \sim 0.023$.

Note that in both the limits the cancellations could only be achieved because of the large value of $\sqrt{\Delta m_{\text{LSND}}^2}$. Cancellations in three generations is not possible because of absence of any term which can counter the large positive value of the first term. This leaves the effective neutrino mass bounded from below in the three generation case.

It is to be noted that in the red shaded region in the right panel of Fig. 7 the value of $m_{\beta\beta}$ is > 0.06 eV, while, the current experimental bound is $m_{\beta\beta} < 0.07$ eV. Therefore, a portion of $m_{\beta\beta}$ is already disfavored for certain parameter values from the current experimental bounds by GERDA and KamLAND-Zen experiments. This experimental bound can constrain the sterile parameter θ_{14} as presented in Fig. 8. In this figure the green shaded zone represents the region allowed by GERDA and KamLAND-Zen in the m_{lightest} vs $\sin\theta_{14}$ plane for the case corresponding to zero Majorana phases of μ-τ reflection symmetry for $3 + 1$ neutrino mixing. We observe that $\sin\theta_{14} < 0.14$ is allowed upto $m_{\text{lightest}} = 0.02$ eV. As m_{lightest} increases further $\sin\theta_{14}$ sharply reduces because higher m_{lightest} is compensated by lower $\sin^2\theta_{14}$ in order to satisfy the upper limit of $m_{\beta\beta}$.

It is well known that near future $0\nu\beta\beta$ experiments like SNO + Phase I[102], KamLAND-Zen 800[103], and LEGEND 200[104] can test the IH region in the context of the three generation scenario. These experiments will be able to test the predictions for $\alpha = \beta = \gamma = 0°$ further. However, in presence of an extra sterile neutrino, a null
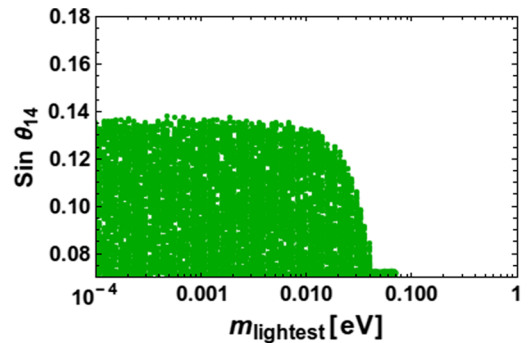

FIG. 8. The effective neutrino mass $m_{\beta\beta}$ for $0\nu\beta\beta$ as a function of $\sin\theta_{14}$.

TABLE II. Predictions for $m_{\beta\beta}$ for various cases for few benchmark points of the lightest neutrino mass (m_1 for NH and m_3 for IH). $m_{\beta\beta\,\mathrm{min}}$ and $m_{\beta\beta\,\mathrm{min}}$ stands for the respective minimum and maximum values of $m_{\beta\beta}$ for each benchmark point.

		$m_{\beta\beta}$ for NH			$m_{\beta\beta}$ for IH		
		$m_1 = 0.001\,\mathrm{eV}$	$m_1 = 0.01\,\mathrm{eV}$	$m_1 = 0.052\,\mathrm{eV}$	$m_3 = 0.001\,\mathrm{eV}$	$m_3 = 0.01\,\mathrm{eV}$	$m_3 = 0.052\,\mathrm{eV}$
Sterile: Majorana	$m_{\beta\beta\,\mathrm{min}} \times 10^{-3}$	10.28	17.01	57.70	56.43	57.19	77.28
Phases = 0	$m_{\beta\beta\,\mathrm{max}} \times 10^{-3}$	42.15	48.40	89.27	86.47	87.37	108.58
Sterile: Majorana	$m_{\beta\beta\,\mathrm{min}} \times 10^{-3}$	8.92	3.82	0.03	0.01	0.02	0.01
Phases = 90°	$m_{\beta\beta\,\mathrm{max}} \times 10^{-3}$	40.94	36.76	20.40	23.68	23.15	24.54
3 Generation	$m_{\beta\beta\,\mathrm{min}} \times 10^{-3}$	0.46	0.76	13.77	14.28	14.50	20.23
	$m_{\beta\beta\,\mathrm{max}} \times 10^{-3}$	4.83	12.10	53.18	50.37	51.40	73.02

signal in these experiments cannot exclude IH because of the occurrence of the cancellation regions.

(ii) Normal hierarchy:

From the first panel of Fig. 7 we observe that for $\alpha = \beta = \gamma = 0°$, the red shaded region, $m_{\beta\beta}$ stays is in the range ∼0.01–0.05 eV rising upto 0.1 eV for higher values of m_{lightest}. For both three neutrino case (region bounded by black lines) and $3 + 1$ neutrino mixing (with $\alpha = \beta = \gamma = 90°$, blue shaded region), complete cancellation in $m_{\beta\beta}$ is seen to occur for NH. The cancellations occur between 0.001 eV to 0.01 eV for three neutrino mixing while it occurs between 0.01 eV to 0.1 eV for $3 + 1$ neutrino mixing. Thus, compared to the three neutrino case the cancellation region for $3 + 1$ neutrino mixing shifts towards higher values of m_{lightest} due to involvement of $m_4 \sim 1$ eV. To analytically understand the salient features of the predictions for $m_{\beta\beta}$ for NH we scrutinize the following limits:

Case 1: For $m_1 \ll \sqrt{\Delta m_{\mathrm{atm}}^2}$ using Eq. (28) and Eq. (27) we obtain

$$m_{\beta\beta} = \left| \sqrt{\Delta m_{\mathrm{atm}}^2}\, t_{13}^2 e^{i2\beta} + \sqrt{\Delta m_{\mathrm{LSND}}^2}\, s_{14}^2 e^{i2\gamma} \right|. \quad (34)$$

In this case for $\alpha = \beta = \gamma = 0°$, the value of $m_{\beta\beta}$ for $t_{13}^2 \sim 0.024$, $s_{14}^2 \sim 0.05$, $\sqrt{\Delta m_{\mathrm{atm}}^2} \sim 0.05$ eV we get $m_{\beta\beta} \sim 0.03$ eV which is in the range obtained in the figure 7. Since $t_{13}^2 \sim s_{14}^2$ and $\Delta m_{\mathrm{atm}}^2 \ll \Delta m_{\mathrm{LSND}}^2$ cancellations are not possible for smaller values of m_1. For $\alpha = \beta = \gamma = 90°$ gives similar results as the $\alpha = \beta = \gamma = 0°$ case which is also corroborated from the figure.

Case 2: Now, when $m_1 \sim \sqrt{\Delta m_{\mathrm{atm}}^2}$ then the expression for the effective mass reduces to

$$m_{\beta\beta} = \left| c_{13}^2 c_{14}^2 \sqrt{\Delta m_{\mathrm{atm}}^2} (c_{12}^2 + s_{12}^2 e^{i2\alpha} + \sqrt{2} t_{13}^2 e^{i2\beta}) \right.$$
$$\left. + \sqrt{\Delta m_{\mathrm{LSND}}^2}\, s_{14}^2 e^{i2\gamma} \right|, \quad (35)$$

$$\approx 0.033 + 0.017 e^{i2\alpha} + 0.002 e^{i2\beta} + s_{14}^2 e^{i2\gamma}. \quad (36)$$

For zero values of the Majorana phases $m_{\beta\beta}$ can reach up to 0.08 eV for $s_{14}^2 = 0.03$. In this limit, cancellations can occur for $\alpha = \beta = \gamma = 90°$ and $s_{14}^2 \sim 0.015$. Note that the predictions for $m_{\beta\beta}$ in the $3 + 1$ picture for zero Majorana phases for higher values of m_{lightest} are already crossing the current experimental values and this can put bound on sterile parameters as in the previous case. Since the values of $m_{\beta\beta}$ upto $m_{\mathrm{lightest}} \sim 0.001$ eV is in the same ballpark as the IH values for three generation scenario, the near future experiments designed to test the 3 generation IH region can also probe this region. For representative purposes we have included the predictions for $m_{\beta\beta}$ for various cases for few benchmark points of the lightest neutrino mass (m_1 for NH and m_3 for IH) in Table II.

In our analysis we have considered $\Delta m_{\mathrm{LSND}}^2 = 1.7$ eV^2 which gives the physical mass of sterile neutrino $m_4 = m_{\mathrm{ph}}^s \sim 1.3$ eV. The cosmic microwave background analysis in $\Lambda_{\mathrm{CDM}} + r_{0.05} + N_{\mathrm{eff}} + m_{\mathrm{eff}}^s$ model using the Planck 2015 data [1] gives the $N_{\mathrm{eff}} < 3.78$ and $m_{\mathrm{eff}}^s < 0.78$ eV [105]. The bounds including other datasets are more stringent than this. As the effective mass in terms of the N_{eff} and physical mass of sterile neutrino is given as $m_{\mathrm{eff}}^s = \Delta N_{\mathrm{eff}}^{3/4} m_{\mathrm{ph}}^s$, where, $\Delta N_{\mathrm{eff}} = N_{\mathrm{eff}} - 3.046$ one gets $m_{\mathrm{ph}}^s < 0.98$ eV at 95% CL.

V. CONCLUSION

To understand the observed pattern of lepton mixing, μ-τ symmetry may play a crucial role as it can be originated from various discrete flavor symmetries. Along with three active neutrinos, presence of one sterile neutrino may have some interesting predictions on neutrino mixing angles and Dirac CP violating phases within the framework of such μ-τ symmetries. Conventional μ-τ permutation symmetry for $3 + 1$ picture is not a phenomenologically viable scenario as it can not explain correct neutrino mixing (since it predicts $\theta_{13} = 0°$). Hence here we have analyzed a simple extension of it, known as μ-τ reflection symmetry, in the context of $3 + 1$ neutrino mixing. We formulate the mass matrix compatible with the lepton mixing matrix which

can give rise to μ-τ reflection symmetry, defined via $|U_{\mu i}| = |U_{\tau i}|$ where $i = 1, 2, 3, 4$. We obtain and plot the correlations connecting the mixing angle θ_{23} and the CP phase δ for the case when sterile phases are assumed to be zero, as well as present the correlation plots with the sterile phases varied in their full range. We find that if we consider total μ-τ reflection symmetry, i.e., $|U_{\mu i}| = |U_{\tau i}|$ is simultaneously satisfied for all the four columns then the mixing angle θ_{23} is confined in a narrow region around $\theta_{23} = 45°$ and δ is restricted around the maximal CP violating values. However, the deviation of θ_{23} from maximal value with the inclusion of the sterile mixing is not sufficient to account for the observed best fit value. This prompts us to consider partial μ-τ reflection symmetry and study the consequences for each column individually.

The equalities $|U_{\mu 1}| = |U_{\tau 1}|$ and $|U_{\mu 2}| = |U_{\tau 2}|$ yield important correlations among the neutrino mixing angle θ_{23} and Dirac CP phase δ. Interestingly we find that the best-fit value for (θ_{23}, δ) shows a good agreement with inverted neutrino mass hierarchy for $|U_{\mu 1}| = |U_{\tau 1}|$ and normal mass hierarchy for $|U_{\mu 2}| = |U_{\tau 2}|$. With precise measurement of θ_{23} and δ in near future there is a clear possibility of verifying these correlations. The inclusion of the sterile CP phases widens the allowed regions. For the equality $|U_{\mu 3}| = |U_{\tau 3}|$ the mixing angle θ_{23} sightly deviates from its maximal value and falls mostly in the lower octant ($\theta_{23} < 45°$) including the effect of sterile mixing angle. This, however, is not supported by the global oscillation analysis [76,77,80]. The equality $|U_{\mu 4}| = |U_{\tau 4}|$ yields an one-to-one correspondence between the sterile mixing angles θ_{24} and θ_{34} making it one of the most significant finding in the present study. So far, there exists only an upper limit on θ_{34}. Interestingly, here we find that the correlation obtained from $|U_{\mu 4}| = |U_{\tau 4}|$ restricts θ_{34} within the range 4.9°–9.8°. The allowed region in the θ_{24}–θ_{34} plane also gets severely restricted. Future experiments sensitive to these mixing angles can test the correlations discussed.

We also explore the possibility of testing the μ-τ reflection symmetry for $3 + 1$ neutrino mixing at the future LBL experiment DUNE. The application of the correlations constrains a significant area of the parameter space yet unconstrained by the present global fit data. In particular the constraint is more stringent for the relation $|U_{\mu 1}| = |U_{\tau 1}|$ and all the CP conserving values $\delta = 0°, 180°, 360°$ are excluded at 3σ. However, for $|U_{\mu 2}| = |U_{\tau 2}|$ CP conserving values of δ remain allowed.

Furthermore, we expound the implications of the μ-τ reflection symmetry for $3 + 1$ neutrino mixing at neutrino-less double β experiments by calculating the effective neutrino mass ($m_{\beta\beta}$) for this scenario. The μ-τ reflection symmetry predicts the Majorana phases to be zero or 90°. For the former predicted effective neutrino mass is higher and can be explored at the future $0\nu\beta\beta$ experiments. In fact for higher values of the lightest neutrino mass the effective neutrino mass $m_{\beta\beta}$ can cross the current experimental bounds when Majorana phases are assumed to be zero. We have shown that, for IH, this constrains the sterile parameter θ_{14} under 8° using the bounds on the effective neutrino mass. For the Majorana phases as 90°, for IH there can be cancellation regions in stark contrast with the three generation predictions. For NH, the cancellation region for the $3 + 1$ case occur for higher values of the lightest neutrino mass as compared to the three neutrino picture.

In conclusion, μ-τ reflection symmetry for sterile neutrinos in a $3 + 1$ picture gives some interesting predictions which can be tested in future neutrino oscillation and neutrinoless double beta experiments and the scenario can be confirmed or falsified.

ACKNOWLEDGMENTS

[1] P. A. R. Ade *et al.* (Planck Collaboration), Astron. Astrophys. **594,** A13 (2016).

[2] S. F. King, J. Phys. G **42,** 123001 (2015).

[3] G. Altarelli and F. Feruglio, Rev. Mod. Phys. **82,** 2701 (2010).

[4] A. Yu. Smirnov, J. Phys. Conf. Ser. **335,** 012006 (2011).

[5] H. Ishimori, T. Kobayashi, H. Ohki, Y. Shimizu, H. Okada, and M. Tanimoto, Prog. Theor. Phys. Suppl. **183,** 1 (2010).

[6] S. F. King and C. Luhn, Rep. Prog. Phys. **76,** 056201 (2013).

[7] P. F. Harrison, D. H. Perkins, and W. G. Scott, Phys. Lett. B **530,** 167 (2002).

[8] S. F. King and C. Luhn, J. High Energy Phys. 09 (2011) 042.

[9] B. Karmakar and A. Sil, Phys. Rev. D **91,** 013004 (2015).

[10] B. Karmakar and A. Sil, Phys. Rev. D **96,** 015007 (2017).

[11] D. Borah and B. Karmakar, Phys. Lett. B **789,** 59 (2019).

[12] Z.-z. Xing and Z.-h. Zhao, Rep. Prog. Phys. **79,** 076201 (2016).

[13] P. F. Harrison and W. G. Scott, Phys. Lett. B **547**, 219 (2002).

[14] G. Altarelli, F. Feruglio, and L. Merlo, Fortschr. Phys. **61**, 507 (2013).

[15] F. P. An *et al.* (Daya Bay Collaboration), Phys. Rev. Lett. **108**, 171803 (2012).

[16] W. Grimus and L. Lavoura, Phys. Lett. B **579**, 113 (2004).

[17] P. M. Ferreira, W. Grimus, L. Lavoura, and P. O. Ludl, J. High Energy Phys. 09 (2012) 128.

[18] W. Grimus and L. Lavoura, Fortschr. Phys. **61**, 535 (2013).

[19] R. N. Mohapatra and C. C. Nishi, Phys. Rev. D **86**, 073007 (2012).

[20] E. Ma, A. Natale, and O. Popov, Phys. Lett. B **746**, 114 (2015).

[21] A. S. Joshipura and K. M. Patel, Phys. Lett. B **749**, 159 (2015).

[22] A. S. Joshipura, J. High Energy Phys. 11 (2015) 186.

[23] A. S. Joshipura and N. Nath, Phys. Rev. D **94**, 036008 (2016).

[24] C. C. Nishi and B. L. Snchez-Vega, J. High Energy Phys. 01 (2017) 068.

[25] Z.-h. Zhao, J. High Energy Phys. 09 (2017) 023.

[26] Z.-C. Liu, C.-X. Yue, and Z.-h. Zhao, J. High Energy Phys. 10 (2017) 102.

[27] Z.-z. Xing, D. Zhang, and J.-y. Zhu, J. High Energy Phys. 11 (2017) 135.

[28] Z.-z. Xing and J.-y. Zhu, Chin. Phys. C **41**, 123103 (2017).

[29] A. S. Joshipura, arXiv:1801.02843.

[30] N. Nath, Z.-z. Xing, and J. Zhang, Eur. Phys. J. C **78**, 289 (2018).

[31] Z.-h. Zhao, Nucl. Phys. **B935**, 129 (2018).

[32] Z.-z. Xing and S. Zhou, Phys. Lett. B **737**, 196 (2014).

[33] K. Chakraborty, K. N. Deepthi, S. Goswami, A. S. Joshipura, and N. Nath, Phys. Rev. D **98**, 075031 (2018).

[34] A. S. Joshipura and K. M. Patel, J. High Energy Phys. 01 (2017) 134.

[35] S.-F. Ge, D. A. Dicus, and W. W. Repko, Phys. Lett. B **702**, 220 (2011).

[36] S.-F. Ge, D. A. Dicus, and W. W. Repko, Phys. Rev. Lett. **108**, 041801 (2012).

[37] C. H. Albright and W. Rodejohann, Eur. Phys. J. C **62**, 599 (2009).

[38] W. Grimus and L. Lavoura, J. High Energy Phys. 09 (2008) 106.

[39] K. N. Abazajian *et al.*, arXiv:1204.5379.

[40] C. Athanassopoulos *et al.* (LSND Collaboration), Phys. Rev. Lett. **77**, 3082 (1996).

[41] A. Aguilar-Arevalo *et al.* (LSND Collaboration), Phys. Rev. D **64**, 112007 (2001).

[42] A. A. Aguilar-Arevalo *et al.* (MiniBooNE Collaboration), Phys. Rev. Lett. **110**, 161801 (2013).

[43] A. A. Aguilar-Arevalo *et al.* (MiniBooNE Collaboration), Phys. Rev. Lett. **121**, 221801 (2018).

[44] M. A. Acero, C. Giunti, and M. Laveder, Phys. Rev. D **78**, 073009 (2008).

[45] J. Kopp, P. A. N. Machado, M. Maltoni, and T. Schwetz, J. High Energy Phys. 05 (2013) 050.

[46] C. Giunti, M. Laveder, Y. F. Li, Q. Y. Liu, and H. W. Long, Phys. Rev. D **86**, 113014 (2012).

[47] G. Mention, M. Fechner, T. Lasserre, T. A. Mueller, D. Lhuillier, M. Cribier, and A. Letourneau, Phys. Rev. D **83**, 073006 (2011).

[48] T. A. Mueller *et al.*, Phys. Rev. C **83**, 054615 (2011).

[49] S. Goswami, Phys. Rev. D **55**, 2931 (1997).

[50] M. Dentler, Á. Hernndez-Cabezudo, J. Kopp, P. A. N. Machado, M. Maltoni, I. Martinez-Soler, and T. Schwetz, J. High Energy Phys. 08 (2018) 010.

[51] C. Giunti and T. Lasserre, arXiv:1901.08330.

[52] B. Dasgupta and J. Kopp, Phys. Rev. Lett. **112**, 031803 (2014).

[53] X. Chu, B. Dasgupta, M. Dentler, J. Kopp, and N. Saviano, J. Cosmol. Astropart. Phys. 11 (2018) 049.

[54] N. Song, M. C. Gonzalez-Garcia, and J. Salvado, J. Cosmol. Astropart. Phys. 10 (2018) 055.

[55] K. N. Abazajian, Phys. Rep. **711–712**, 1 (2017).

[56] J. Barry, W. Rodejohann, and H. Zhang, J. High Energy Phys. 07 (2011) 091.

[57] J. Barry, W. Rodejohann, and H. Zhang, J. Cosmol. Astropart. Phys. 01 (2012) 052.

[58] D. C. Rivera-Agudelo and A. Prez-Lorenzana, Phys. Rev. D **92**, 073009 (2015).

[59] A. Merle, S. Morisi, and W. Winter, J. High Energy Phys. 07 (2014) 039.

[60] D. Borah, Phys. Rev. D **95**, 035016 (2017).

[61] N. Sarma, K. Bora, and D. Borah, Eur. Phys. J. C **79**, 129 (2019).

[62] C. C. Nishi, Phys. Rev. D **93**, 093009 (2016).

[63] N. Nath, Phys. Rev. D **98**, 075015 (2018).

[64] N. Nath, arXiv:1808.05062.

[65] C. C. Nishi, B. L. Snchez-Vega, and G. S. Silva, J. High Energy Phys. 09 (2018) 042.

[66] W. Rodejohann and X.-J. Xu, Phys. Rev. D **96**, 055039 (2017).

[67] P. Chen, G.-J. Ding, F. Gonzalez-Canales, and J. W. F. Valle, Phys. Lett. B **753**, 644 (2016).

[68] Y.-L. Zhou, arXiv:1409.8600.

[69] H.-J. He, W. Rodejohann, and X.-J. Xu, Phys. Lett. B **751**, 586 (2015).

[70] H.-J. He and X.-J. Xu, Phys. Rev. D **86**, 111301 (2012).

[71] S.-F. Ge, H.-J. He, and F.-R. Yin, J. Cosmol. Astropart. Phys. 05 (2010) 017.

[72] H.-J. He and F.-R. Yin, Phys. Rev. D **84**, 033009 (2011).

[73] N. Nath, Phys. Rev. D **99**, 035026 (2019).

[74] S. T. Petcov and A. V. Titov, Phys. Rev. D **97**, 115045 (2018).

[75] I. Girardi, S. T. Petcov, and A. V. Titov, Nucl. Phys. **B911**, 754 (2016).

[76] N. 3.2, (2018), www.nu-fit.org.

[77] I. Esteban, M. C. Gonzalez-Garcia, A. Hernandez-Cabezudo, M. Maltoni, and T. Schwetz, J. High Energy Phys. 01 (2019) 106.

[78] S. Gariazzo, C. Giunti, M. Laveder, and Y. F. Li, J. High Energy Phys. 06 (2017) 135.

[79] P. F. de Salas, D. V. Forero, C. A. Ternes, M. Tortola, and J. W. F. Valle, Phys. Lett. B **782**, 633 (2018).

[80] F. Capozzi, E. Lisi, A. Marrone, and A. Palazzo, Prog. Part. Nucl. Phys. **102,** 48 (2018).

[81] P. Ballett, S. F. King, S. Pascoli, N. W. Prouse, and T. Wang, Phys. Rev. D **96,** 033003 (2017).

[82] K. Abe *et al.* (Super-Kamiokande Collaboration), Phys. Rev. D **91,** 052019 (2015).

[83] M. G. Aartsen *et al.* (IceCube Collaboration), Phys. Rev. D **95,** 112002 (2017).

[84] P. Adamson *et al.* (MINOS Collaboration), Phys. Rev. Lett. **117,** 151803 (2016).

[85] P. Adamson *et al.* (NOvA Collaboration), Phys. Rev. D **96,** 072006 (2017).

[86] K. Abe *et al.* (T2K Collaboration), Phys. Rev. D **99,** 071103 (2019).

[87] R. Gandhi, B. Kayser, S. Prakash, and S. Roy, J. High Energy Phys. 11 (2017) 202.

[88] A. De Gouva, K. J. Kelly, G. V. Stenico, and P. Pasquini, Phys. Rev. D **100,** 016004 (2019).

[89] A. Ghoshal, A. Giarnetti, and D. Meloni, arXiv: 1906.06212.

[90] P. Coloma, D. V. Forero, and S. J. Parke, J. High Energy Phys. 07 (2018) 079.

[91] P. Huber, M. Lindner, and W. Winter, Comput. Phys. Commun. **167,** 195 (2005).

[92] P. Huber, J. Kopp, M. Lindner, M. Rolinec, and W. Winter, Comput. Phys. Commun. **177,** 432 (2007).

[93] J. Kopp, M. Lindner, and T. Ota, Phys. Rev. D **76,** 013001 (2007).

[94] M. C. Gonzalez-Garcia and M. Maltoni, Phys. Rev. D **70,** 033010 (2004).

[95] G. Fogli, E. Lisi, A. Marrone, D. Montanino, and A. Palazzo, Phys. Rev. D **66,** 053010 (2002).

[96] R. Gandhi, P. Ghoshal, S. Goswami, P. Mehta, S. U. Sankar, and S. Shalgar, Phys. Rev. D **76,** 073012 (2007).

[97] A. Gando *et al.* (KamLAND-Zen Collaboration), Phys. Rev. Lett. **117,** 082503 (2016); **117,** 109903(E) (2016).

[98] M. Agostini *et al.* (GERDA Collaboration), Phys. Rev. Lett. **120,** 132503 (2018).

[99] C. Alduino *et al.* (CUORE Collaboration), Phys. Rev. Lett. **120,** 132501 (2018).

[100] S. Dell'Oro, S. Marcocci, M. Viel, and F. Vissani, Adv. High Energy Phys. **2016,** 2162659 (2016).

[101] K. N. Vishnudath, S. Choubey, and S. Goswami, Phys. Rev. D **99,** 095038 (2019).

[102] V. Lozza, *Magellan Workshop, Hamburg, Germany, 2016* (Magellan Workshop, Hamburg, 2016), pp. 8794.

[103] J. Shirai, https://www.iopconferences.org/IOP/media/uploaded/EVIOP/event_948/09.45__5__Shirai.pdf.

[104] J. Myslik (LEGEND Collaboration), in *13th Conference on the Intersections of Particle and Nuclear Physics (CIPANP 2018) Palm Springs, California, USA, 2018* (2018), https://conferences.lbl.gov/event/137/session/17/contribution/210/material/slides/0.pdf.

[105] S. R. Choudhury and S. Choubey, Eur. Phys. J. C **79,** 557 (2019).